Absolute Photometric Calibration of Detectors to 0.3 mmag Using Amplitude-Stabilized Lasers and A Helium-Cooled Absolute Radiometer

Peter J. Miller

Cambridge Research and Instrumentation, Inc., Cambridge, MA

Short Title: Absolute Detector Calibration using Lasers and a Radiometer

Section 1: Abstract

We describe laser sources whose intensity is determined with a cryogenic electrical substitution radiometer. Detectors are then calibrated against this known flux, with an overall error of 0.028% (0.3 mmag). Ongoing research at C.R.I. has produced laser intensity stabilizers with flicker and drift of < 0.01%. Recently, the useful wavelength limit of these stabilizers has been extended to 1.65 microns by using a new modulator technology and InGaAs detectors. This will allow improved characterization of infrared detector systems. We compare data from a Si photodiode calibration using the method of Zalewski and Geist against an absolute cavity radiometer calibration, as an internal check on the calibration system.

Section 2: Introduction

Liquid helium cooled electrical substitution radiometers have been developed in order to realize the higher accuracy, lower noise floor, and faster time response which cryogenic operation provides[1 - 4]. Their high absolute accuracy has been demonstrated at the NPL through direct measurement of the Stefan-Boltzmann constant, and by comparison with emission from the BESSY source. The absolute error of these devices is estimated at 0.01%. We have constructed a calibration facility based upon a cryogenic absolute radiometer, whose optics have been optimized for use with collimated laser sources. The radiometer is discussed in Section 4.

In a laser-based calibration, the radiometer optics are greatly simplified, with a corresponding increase in accuracy. In particular, corrections for aperture size indeterminacy, for diffraction, for

scattered light, and for spectral variations are reduced to negligible size (< 1 ppm). However, in order to realize the high accuracy which a helium-cooled radiometer offers, the intensity of the laser source must be stable to the same high degree. Accordingly, we have developed laser amplitude stabilizers which use feedback control techniques to stabilize the intensity of laser sources to better than 0.01 percent over one hour. Further, these stabilizers can now stabilize infrared lasers, to wavelengths of at least 1.52 microns. They are described in Section 3.

The overall calibration system is diagrammed in Figure 1, and consists of a bank of laser sources; a laser stabilizer; a detector wheel which contains the device(s) to be calibrated; and the cryogenic radiometer (see Figure 1). In order to calibrate a detector at a particular power level and wavelength, the appropriate laser is selected and the rough power level selected by the use of neutral density filters and adjustments to the laser itself. The beam passes through a laser intensity stabilizer, which is used to select the exact operating intensity level. A reading is then taken with the device being calibrated.

When the device response has been measured, the detector wheel is rotated to let the beam pass through to the cryogenic radiometer. A reading of the beam power is then made by the radiometer, which takes approximately two minutes. The responsivity of the device is given by the device response divided by the beam power, as determined by the radiometer. If needed, a detector dark count reading can be made while the beam power is being measured by the radiometer; conversely, the dark count reading required by the radiometer is made while the

detector response is being measured.

Note that this calibrates the detector's radiometric response, but since a monochromatic source is used, a photometric calibration may be easily derived from it. The two calibrations are related by the energy per photon at the wavelength of calibration; since that wavelength is known to 7 digits or more, there is no error suffered through this practice. The calibration procedure and the system performance are described in Section 5, following a detailed description of the individual components.

Section 3: The stabilized laser source

Lasers are underutilized in the calibration world. Their high specific radiance, monochromaticity, excellent beam profile, ease of collimation, and ease of use recommend them for many photometric measurements. However, they are intrinsically unstable in their power output, exhibiting fluctuations of a few percent. Laser designers seek to minimize these fluctuations, but their efforts are hampered by the fact that lasers are designed to be runaway oscillators.

We have developed a commercial line of laser intensity stabilizers which operate outside of the laser itself, based on work done at the Bureau of Standards[5]. Figure 2 is a block diagram of one of these units. Light from the unstabilized laser passes through an input polarizer, which linearly polarizes it. The light then passes through a Pockels' cell, which is a voltage-controlled waveplate. Depending on the applied voltage, the polarization axis of the light is rotated by an angle between 0 and 90 degrees. Next, the light passes through a second, exit polarizer; the fraction of the light transmitted

through this polarizer depends on the amount of rotation produced by the Pockels' cell. As this demonstrates, the polarizers and Pockels' cell form a voltage-controlled attenuator.

A fraction of the exiting light is sampled by a beamsplitter, and directed onto a precision photodiode. The signal from this monitor photodiode is sent to a high-stability preamplifier and then into a servo amplifier. The servo amplifier seeks to keep this monitor signal absolutely constant, by altering the state of the voltage-controlled attenuator. If the exiting beam flux decreases slightly, the servo drives voltage-controlled attenuator to higher transmission, until the exiting signal is once again at the desired level. Similarly, a bright flicker in the laser will evince a compensating decrease in attenuator transmission. The servo loop gain is 35,000, and the servo bandwidth is 300 kHz.

The improvement in stability this produces is shown dramatically in Figures 3 and 4. Figure 3 shows the output power of a 2 mW Jodon He-Ne laser producing linearly polarized light at 632.89 nm, without intensity stabilization. This is a one hour time series measured by a windowless Hammamatsu Si photodiode, model number 1336, preamplified by a custom circuit with short-term noise and drift of < 50 ppm. A bar denoting a 1 mmag variation is drawn for scale, and the rms deviaton of this data is 1.18 percent.

Figure 4 shows the improvement brought about by stabilizing this laser with one of our stabilizers. Otherwise, the experimental setup is the same. Again, a bar denoting a 1 mmag variation is drawn for scale. This beam has an rms deviation of 0.010 percent (0.1 mmag) over one hour. Such a source is stable enough for nearly all calibra-

tion tasks, and is much more convenient to use than extended sources such as blackbodies or lamp and monochromator systems.

Further data are presented in Figures 5 and 6. The former shows the data of Figure 4, replotted on a much expanded vertical scale. Again, a bar denoting 1 mmag variation is drawn for scale, and the data spans one hour. Figure 6 shows the output of a laser diode operating at 838 nm, stabilized by the same stabilizer. This laser diode chip is made by Sharp and is sold by D.O. Industries in a housing with a power supply and collimating optics; it provides a 1.2 mm beam with < 1 mrad divergence and up to 25 mW output power. Laser diodes are particularly useful, as they are inexpensive, reliable, easy to use, and available at a variety of wavelengths betweeen 710 nm and 1.3 microns.

It is worth noting that the previous data were taken by an external detector placed in the stabilized beam path. Earlier work using commercial 'noise-eater' stabilizers gave temptingly good stability at the monitor photodiode signal, but poor stability in the exiting beam. This led some researchers to conclude that stabilizers could not be of use in a precision photometric program. Deficiencies in these units included poor beamsplitter design and insufficient polarization by the exit polarizer. In addition to addressing these problems, our present generation of stabilizers servo-control the temperature of the monitor photodiode, which improves the performance when working in the ultra-violet and infrared.

Finally, a recent development has extended the wavelength range of these units to beyond 1.523 microns. Pockels' cells are not readily available for use beyond 1.2 microns, and silicon photodiodes lose all

responsivity at wavelengths longer than 1.15 microns. We have developed a variable retardance cell which operates to 2.0 microns. By changing from silicon detectors to InGaAs, we can now operate at wavelengths up to the cutoff for that detector. A block diagram for an infrared stabilizer is given in Figure 7. The InGaAs detectors are not as linear or spatially uniform as the excellent Si devices now available. Because of the lower quality of the infrared detectors, when working with laser sources at wavelengths beyond 1.15 microns, the stabilized light has an rms variation of 0.05 percent. A list of the laser sources we have stabilized, the operating wavelengths and resultant stabilities is given in Table 1.

Section 4: The helium-cooled radiometer

A radiometer which measures flux by application of an electical power so as to exactly balance a radiant power is termed an electrical substitution radiometer (ESR). There is a well-established art to making these instruments, and a complete literature dedicated to the modelling and characterization of their properties[6, 7]. Ambient temperature devices have flown on a number of space missions, monitoring earth radiation and measuring the solar constant[8]. The suitability of these radiometers for high-precision measurements is well-established. However, they suffer several limitations, which can best be explained by describing their operation in detail.

An ESR is diagrammed in Figure 8. It consists of a receiver cone with a heater and thermometer integrally bonded to it; a heat link connecting this part to a heat sink; and the fixed-temperature heat sink. Note that all wiring to the heater and to the thermometers has

been omitted in this drawing. Surrounding this assembly are radiation shields and apertures. Light incident on the reciever cone is absorbed by black paint on its surface, raising the temperature of the receiver above that of the heat sink. The temperature rise is given by the flux F_0 times the thermal impedance of the heat link. When the temperature has equilibrated, it is read by the thermometer at the receiver. The light flux is then removed by e.g. closing a shutter, and heat is applied by the electrical heater until the same temperature is obtained. If the heat flow paths are identical for electrical and radiant power inputs, this temperature is achieved when the electrical and radiant power levels are identical, and an absolute determination of radiant flux has been made.

Of course, there are differences in the temperature distributions realized under these two heating modes. To the extent that these differences cause the receiver thermometer to respond differently to heater power and radiant power, there is said to be a nonequivalence between electrical and radiant response. Such a nonequivalence directly affects the absolute accuracy of the radiometer. These nonequivalence can be minimized by increasing the conductivity of the receiver, so as to make it a better isotherm. Similarly, if there is power dissipation in these leads during the electrical phase of the measurement, it will result in a nonequivalence term. It is important to note that this in no way limits the usefulness of these instruments in applications where only precision is required, but it sets a limit on the accuracy of the resultant measurements.

The magnitude of this error can be diminished by operation at cryogenic temperatures. For high quality metals, thermal conductivity

increases until the electron mean free path exceeds the crystal grain size. This condition is met, for high-purity annealed samples, at approximately 10 K, where they exhibit a conductivity more than 10 times the room temperature value. More striking is the decrease in thermal capacity, described to good accuracy by the Debye law as proportional to the cube of the temperature. Thus, a sample at 4.2 K would have a capacity 0.003 percent of its room temperature value. In practice, the figure is closer to 0.1 percent, which is still dramatic. This permits the cone to be thick-walled without having a large heat capacity. Thus, excellent isotherms can be had without overly slow response.

In addition to these two factors, any nonequivalence due to power dissipation in the heater leads is vanishes when NbTi superconducting wire is used for the leads. Finally, stray heat transport by radiation and convection are greatly decreased by operating the radiometer within a liquid-helium enclosure at ultra-high vacuum. It is possible to resolve heat inputs of approximately 1 nW. This is roughly the flux of a 7-th magnitude star observed through the 4-meter Kitt Peak telescope, so even a cryogenic radiometer is not suitable for direct observation. Nonetheless, it extends the flux range down closer to that necessary for astronomical work, so that transfer calibrations may be performed.

The cryogenic radiometer used in our calibration system is diagrammed in Figure 9. Light enters through a Brewster's angle window, and passes through radiation shields at 77K and 10K before landing on the receiver cone. All apertures are 8 mm in diameter, and the receiver itself has a 1 cm active area. The receiver itself is a long

tube of OFHC copper with an oblique bottom plate. In this way, there is no troublesome "point", as there is with a cone-type geometry; absorptivity of 0.999920 is achieved, with the residual 80 ppm arising from retro-reflection. The system time constant is 20 seconds, with a nominal operating power of 1.0 mW. Receivers have been tested with nominal operating power levels as low as 20 microwatts, and time constants as short as 0.6 seconds.

The error analysis and performance specifications for this radiometer are given in Tables 2 and 3. Table 2 gives the full energy balance equation for the radiometer, including convective, conductive, and radiative transport terms. In addition, the nonequivalence factor is defined, using primed variables to denote values observed under electrical heating and unprimed variables to denote values seen under radiant heating. Looking ahead to the values in Table 3, we see that many of these terms in equations [1] and [2] can be omitted to yield a simpler equation [3]. An overall error budget for the radiometer is performed in Table 3. The rms variance is estimated at 0.018 percent, due largely to DMM limitations and uncertainty in the Brewster angle window transmission.

An upper limit on the instrument's nonequivalence was had by winding a second heater on the receiver, placed so as to deposit its heat in a very different pattern from that obtained under radiant heating. This ought to maximize the nonequivalence arising from changing heat conduction between the radiant and electrical heating phases. This experiment produced a null result at the 0.02 percent level, limited by the resolution of the DMM used.

Section 5: Calibrations using the complete system

We have calibrated several silicon photodiodes against the radiometer using stabilized He-Ne and Argon ion laser sources. Calibrations against the radiometer can be performed at any wavelength between 260 nm and 2.0 microns, limited by the transmission of the fused silica used for the Brewster angle window. Power levels from 0.1 mW to 2 mW may be made directly, with extensions beyond this range by use of calibrated beamsplitters and attenuators.

The procedure was outlined earlier, and it consists of shining a stabilized laser source onto the device to be calibrated, mounted on a detector wheel. The detector response is noted, and then the detector wheel is rotated to let light pass through to the radiometer. During this phase, a dark reading is taken on the device being calibrated. This is the radiant phase of a radiometer measurement. Once the receiver equilibrates, the temperature is noted, and the detector wheel is rotated back. Once again the laser beam lands on the detector being calibrated. Electrical heating is applied to the receiver cone until the receiver cone temperature matches the earlier reading. The cone heater power is noted, as it should exactly equal the radiant flux.

Data from several calibrations of a single Si diode are presented in Figure 10 and 11. Figure 10 shows the radiometer response to a stabilized He-Ne laser beam, measured several times. If the beam were absolutely stable, this only variations would be those due to the radiometer readout noise. In fact, the rms variation of this data is 0.018 percent, which is nearly identical to the figure derived from the formal error budget (0.019 percent). This implies that our formal

error budget overestimates the actual error, as there is a 0.01 percent contribution from variation from variations in the beam power, which predicts a total error of 0.020 percent.

Each point represents approximately 200 seconds of integration by the radiometer. Note that for an instrument with a 20 second time constant, this is 10 ↑, which may lead the reader to conclude that we are waiting for the sytem to come to thermal equilibrium. Actually, we use servo techniques to achieve an effective time constant of 1 second, so 0.01 percent measurements can be made in 10 seconds. We use a longer dwell time to reduce thermometry noise, which must be reduced to a few microkelvin.

Figure 11 shows the response of a windowless Hammamatsu model 1336 diode to the same stabilized beam. If the stabilized beam were perfect, the only variations would be those due to the detector nonuniformity and noise. The nonuniformity term occurs because the beam did not always land on the same portion on the detector. Detector noise is vanishing for these devices, so the rms variation of 0.032 percent in the data implies that spatial nonuniformity in the diode responsivity is the dominant source of the variations.

To complete the calibration, one simply divides the device response by the beam power. Before presenting this data, we note that there is an independent calibration we have performed which functions as a check on the radiometric calibration. Specifically, we have performed the method of diode self-calibration, developed by Zalewski and Geist[9-11]. This method involves measuring a series of correction factors based on a model of the internal device physics of silicon photodiodes; in this way, one can determine the absolute responsivity

of a diode detector.

This self-calibration is observed to be destructive to some devices[12], so we performed it after the radiometer calibration is complete[13]. The Zalewski and Geist self-calibration value is presented along with the radiometer calibration values, in Figure 12. Again, each radiometer value corresponds to a single radiant/electrical cycle of the radiometer, and a single diode reading. The variance between the radiometer values is 0.028 percent, and the mean of the radiometer values agrees with the self-calibration value to within 0.01 percent.

It is interesting to note that the variance between successive responsivity values is lower than the variance between diode readings, which is 0.032 percent. This implies that there is some correlation between the variations in the diode readings and variations in the radiometer readings, as variations in the ratio are lower than in one of the terms. The obvious meaning of this is that both the diode and the radiometer are detecting drift in the stabilized laser beam, at roughly the 0.01 percent level. Since detecting varying light levels is the primary function of detectors, both diodes and radiometers, this is hardly a shocking result.

Section 6: Summary

Results are summarized in Table 4. We have demonstrated stabilized laser sources with intensity variations of less than 0.010 percent over an hour. We have demonstrated a helium-cooled ESR absolute radiometer with a standard error of 0.018 percent, and used it to calibrate diode photometric detectors. An independent calibration of

a silicon diode was made using a technique based on the internal device physics, and agreement was found to within 0.010 percent. Capability was described for calibrating sources over the spectral range 280 nm - 1.6 microns, and over the power range 0.1 mW - 2 mW. This capability is felt to be of most importance for devices which need absolute calibration to maintain stability over a long time, and which lack a self-calibration.

Acknowledgements

This work was supported in part by N.B.S. contract #43NANB613437.

References

1) P. Foukal and P. Miller, Final Report on NOAA contract NAS0RAC00204, 1982.

2) P. Foukal and P. Miller, SPIE Proceedings, 416, 197, 1983.

3) P. Foukal, C. Hoyt, and P. Miller, Advances in Absolute Radiometry, Proceedings, 1985.

4) N. Fox, Advances in Absolute Radiometry, Proceedings, 1985.

5) J. Geist, M.A. Lind, A.R. Schaefer, and E.F. Zalewski, NBS Technical Note 954, 1977.

6) H. Jacobowitz, H.V. Soule, H.L. Kyle, F.B. House, and Nimbus-7 ERB Experiment Team, J. Geophys. Res., 89, 5021-5028, 1984.

7) J.R. Mahar, Interim Report to NASA on Contract NASA-1-18106, 1987.

8) R.C. Willson, Applied Optics, 18, 179-188, 1979.

9) E.F. Zalewski and J. Geist, Applied Optics, 19, 1214-1216, 1980.

10) A.L. Schaefer, E.F. Zalewski, and J. Geist, Applied Optics, 22, 1232-1236, 1983.

11) J. Geist, E.F. Zalewski, and A.R. Schaefer, Applied Optics, 19, 3795-3799, 1980.

12) J. Verdebout, Applied Optics, 23, 4339, 1984.

13) As an aside, we do not find any degradation when Hammamatsu diodes are calibrated; they require much lower voltages for the front oxide loss measurement than do the E.G.& G. devices which have been reported to exhibit degradation.

Author Address List

Miller, Peter J.

Cambridge Research and

Instrumentation, Inc.

21 Erie Street

Cambridge, MA 02139.

Table 1. Presently available calibration wavelengths.

Wavelength	Laser Source	Stability (est.)
325.0 nm	He-Cd laser	0.04 %
351.1 nm	Ar ion laser	0.04 %
363.8 nm	Ar ion laser	0.04 %
442.5 nm	He-Cd laser	0.028 %
457.9 nm	Ar ion laser	0.028 %
488.0 nm	Ar ion laser	0.028 %
514.5 nm	Ar ion laser	0.028 %
528.7 nm	Ar ion laser	0.028 %
532.0 nm	Nd:YAG (doubled)	0.028 %
632.9 nm	He-Ne laser	0.028 %
838.0 nm	GaAlAs diode laser	0.028 %
1064 nm	Nd:YAG laser	0.028 %
1153 nm	IR He-Ne laser	0.06 %
1318 nm	Nd:YAG laser	0.06 %
1523 nm	IR He-Ne laser	0.06 %

Table 2. Radiometer Error Analysis

The radiometer equations are:

$$(TF_0 + I_s \quad a) + F_{bbs} + F_{rad} + F^{+}_{conv} = F_{bbr} + F_{cond} + F^{-}_{conv}. \qquad [1]$$

$$F'_{bbr} + F'_{cond} + F^{-}_{cond} = E_h I_h. \qquad [2]$$

where:

	=	cone absorptivity
T	=	Brewster angle window transmission
F_0	=	radiant flux
I_s	=	primary scatterer surface intensity
a	=	scattering solid angle
F_{bbs}	=	black body radiation from shields to receiver
F_{rad}	=	black body radiation from window onto receiver
F^{+}_{conv}	=	convective heat transport from cryostat to receiver
F_{bbr}	=	black body radiation from receiver to surroundings
F_{cond}	=	conductive heat flow from receiver to heat sink
F^{-}_{conv}	=	convective heat transport form receiver to cryostat

Unprimed variables denote values observed during radiative heating.

Primed variables denote values observed when during electrical heating.

When F_0 is in the mW range, an excellent approximation to Eq's 1 and 2 is

$$(TF_0 + I_s \quad a) + F_{rad} + F^{+}_{conv} = F_{cond} = E_h I_h \qquad [3]$$

Table 3. Radiometer Error Terms

Term	Magnitude	Std. Error	Percent Error (0.4 mW signal)
	0.99992	10 ppm	0.001
T	0.99970	0.00008	0.008
I_s	0.002 F_0	0.001 F_0	0.00008
a	0.0025	0.0008 Sr	
F_{bbs}	0.1 uW	100 pW	0.000025
F_{rad}	3.0 uW	30 nW	0.0075
F^+_{conv}	5 uW	20 nW	0.005
I_h	1.0 mA	0.01 uA	0.01
E_h	0.4 V	40 uV	0.01

Solving for the probable system error using Equation [3], we obtain:

F_0 = 0.0186 %

Table 4. Capabilities of Laser/Cryogenic Radiometer Calibration

* Absolute calibration - permits long-term studies free of drift.

* Non-contact calibration - nondestructive of device being measured.

* Independant of device physics. Allows calibration of devices which cannot be easily modelled or compensated.

* Device is calibrated outside of radiometer - no size or environmental restrictions are placed on detector.

* Wide spectral range. Present system covers 280 nm - 1.6 microns, but 244 nm - 10.6 microns is possible.

* Laser sources with excellent beam profile and low diffraction, simplifies calibrations, compared to lamp or blackbody sources.

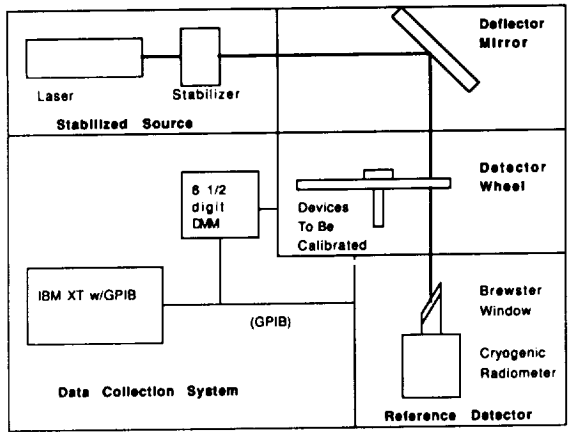

Figure 1. The detector absolute calibration system. Light from the stabilized laser is presented to the cryogenic reference detector or to the detector being calibrated.

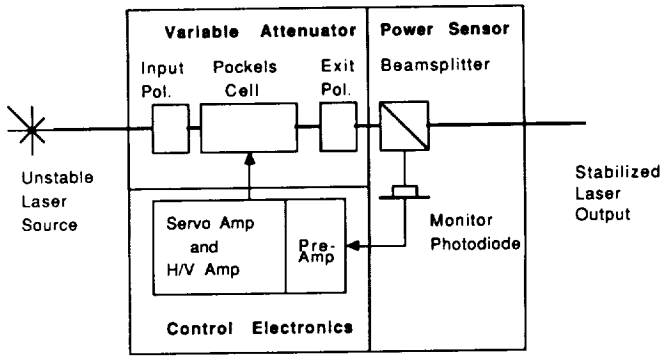

Figure 2. Laser stabilizer block diagram. Light from an unstabilized laser source is passed through an electrically variable attenuator. The setting of the attenuator is servo-controlled so as to keep a fixed power level at the output.

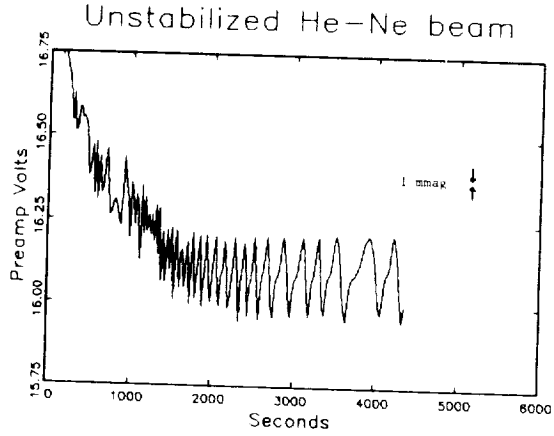

Figure 3. Intensity variations in a He-Ne laser, without stabilization. The readings are taken by a Hammamatsu 1336 windowless Si diode. This test spans approximately 1 hr, and the laser is a linearly polarized Jodon laser operating at 632.899 nm. The periodic variations in power level are probably due to thermal expansion of the laser cavity, which shifts the cavity resonances across the gain envelope of the atomic line which is emitting. The rms variation is 1.19%, and a bar representing a 1 milli-magnitude variation is drawn for scale.

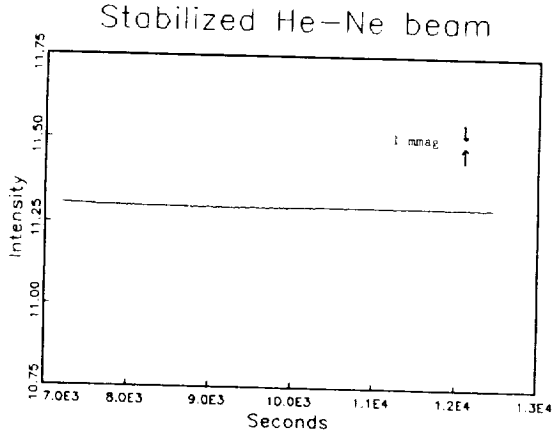

Figure 4. Intensity variations in a He-Ne laser, with stabilization. The laser is identical to those of the previous Figure. These readings were taken by a Hammamatsu 1336 windowless Si diode placed in the stabilized beam. For this data, the rms variation is 0.010%.

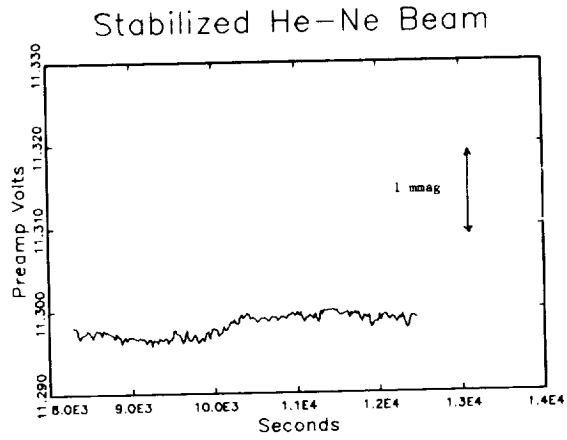

Figure 5. Intensity variations in a He-Ne laser, with stabilization. This is the data from Figure 4, redrawn on an enlarged scale. A bar representing a 1 milli-magnitude variation is drawn for scale.

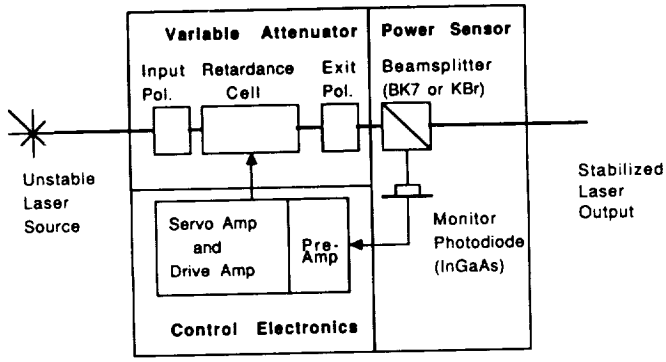

Figure 6. Intensity variations in an 838 nm solid-state diode laser. This test spans 1 hr, and the laser being stabilized is a D.O. Industries 25 mW laser with integral collimated optics; the laser diode chip itself is a Sharp device. The rms variation is 0.002%, and a bar representing 1 mmag variation is shown for scale.

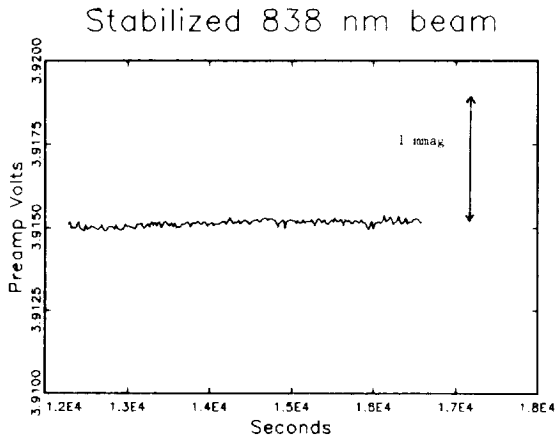

Figure 7. Block diagram of the infrared laser stabilizer. Note that the design closely corresponds to the stabilizer diagrammed in Figure 2, except for the modulator and detector. A retardance cell replaces the Pockels cell, and the monitor photodiode is made of InGaAs, not Si.

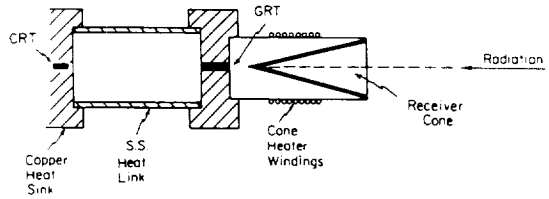

Figure 8. Diagram of the cryogenic radiometer receiver. Light incident on the cone raises the temperature of the cone assembly above that of the heat sink it is attached to. This temperature is noted, and then the light is shuttered and electrical power deposited via the heater to achieve the same temperature. By this substitution of electrical power for radiative power, an absolute reading of incident flux is made.

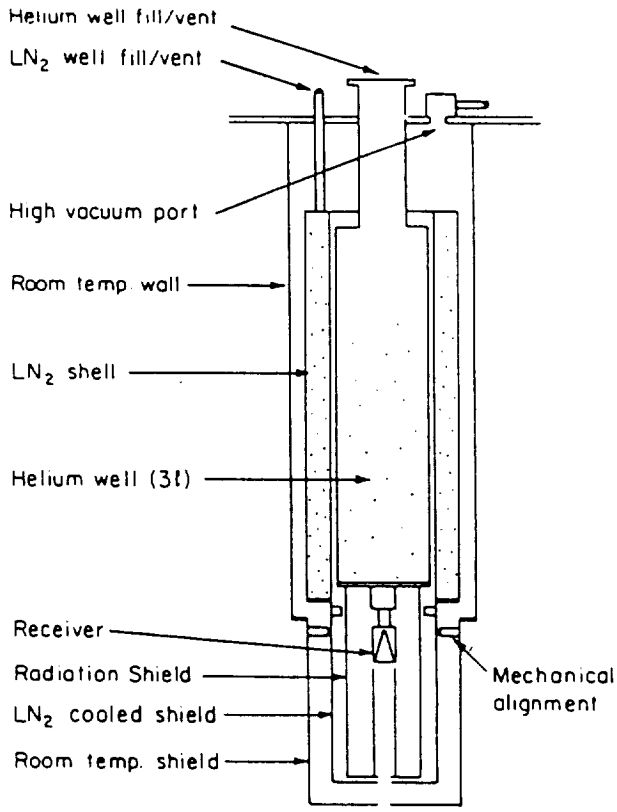

Figure 9. The cryogenic radiometer assembly. Light enters at the bottom, through a Brewster angle window (omitted for clarity), and passes through the LN_2 shield and He-cooled radiation shield on its way to the receiver cone. Liquid helium in the central well cools the heat sink and receiver assembly to 4.2 K or lower.

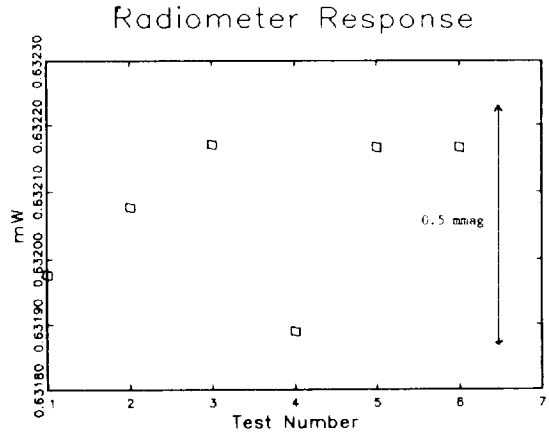

Figure 10. Radiometer response to a stabilized He-Ne laser. Each point represents one reading taken by a substitution of electrical power for the radiative power of the beam, and includes approximately 100 seconds of integration of the radiometer signal. The rms variation is 0.018%, and a bar representing a 0.5 mmag variation is drawn for scale.

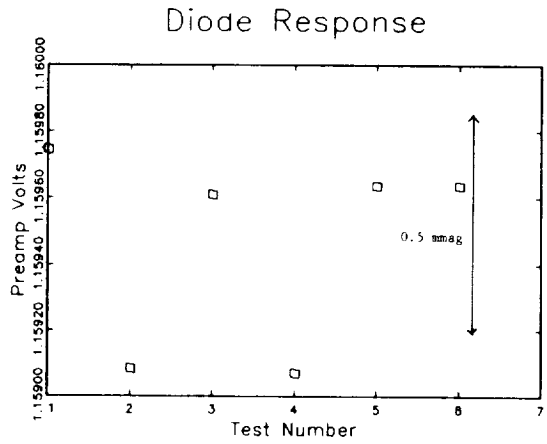

Figure 11. Response of a Hammamatsu 1336 windowless Si diode to a stabilized He-Ne laser beam. These readings were interleaved between successive readings shown in Figure 10. The readings were separated by approximately 2 minutes from the associated radiometer reading. The rms variation of this data is 0.032%, which exceeds the variation in the radiometer readings and in the stabilized source intensity. The excess variation may reflect spatial inhomogeneities across the photodiode face, as the beam illuminated slightly different portions of the diode face on successive readings.

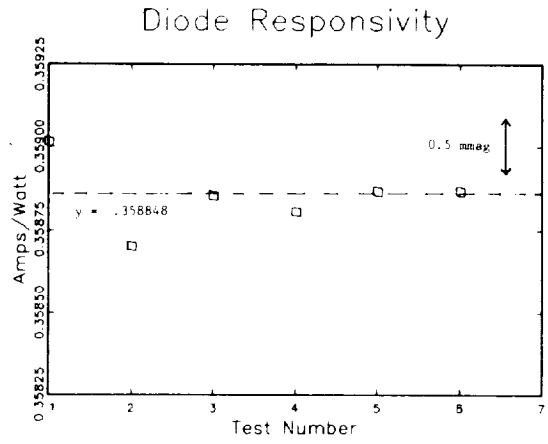

Figure 12. The diode responsivities calculated from Figures 10 and 11. The observed diode current is divided by the radiometer reading of beam power to determine the diode responsivity. The dashed line represents the diode responsivity calculated independently using the self calibration method of Zalewski and Geist. The rms variation of responsivity values is 0.028% (0.3 mmag), while the mean of the population agrees with the independently determined value to within 0.010%.